Lockheed Missiles & Space Company, Inc.
SUNNYVALE, CALIFORNIA

IMAGING THE MAGNETOSPHERE IN THE EXTREME ULTRAVIOLET

Final Report
NASA Contract NASW-4529
NASA Headquarters, Washington, D.C.

Date: **Febuary 6, 1993**

Principal Investigator:
Dr. Y.T. Chiu, (415)-424-3421

Lockheed Palo Alto Research Laboratory
Space Sciences Laboratory, Dept. 91-20, B255
3251 Hanover St., Palo Alto, CA 94304

Contents

1. Objectives of Research

This is the final report on 2.5 calendar years of contract research on magnetosphere imaging in the extreme ultraviolet. The objectives of the research contract can be summarized in three related items:

Objective 1: Investigate the feasibility of the EUV imaging concept by using Lockheed in-situ ion measurement data.

Objective 2: Investigate the technical resources required to make scientific interpretations of such EUV images by end-to-end simulations of the imaging concept.

Objective 3: Construct and test the key element for EUV magnetosphere imaging, the multilayer mirror with normal-incidence reflectance designed for the selected solar resonance line.

2. Accomplishments

Researches as per contract have successfully fulfilled all three scientific objectives stated above. The body of this report emphasizes accomplishments in the second year. Accomplishments in the first year are summarized in the Annual Progress Report for 1991, which is included here as Appendix 1.

Objective 1: Early in the contract period we published a paper on the feasibility of magnetosphere imaging in the EUV in the Geophysical Research Letters (Chiu et al., 17, 267; see Exhibit 1 in Appendix 1). Subsequently, we follow up the work with a more detailed work which has been accepted by Planetary and Space Science (see Exhibit B of this report). Both papers are now referenced repeatedly by workers in the field of EUV imaging of the magnetosphere. Instrument groups are now using its results to determine source requirements for instrument design proposals for NASA's prospective Small Explorer and Inner Magnetosphere Imager missions.

Objective 2: Unlike the more straight forward estimates of photon-counts based on in-situ ion flux data for accomplishing Objective 1, this objective is much more difficult. It attempts to answer the question: How does one convert morphological features of EUV photon images into ion distributions? Here, subtle effects such as Doppler shifts due to thermal and non-thermal ion motion in a magnetic field become important and must be simulated. Such simulations require considerable computational

resources and are accomplished in 1992. The result is a paper recently submitted to the Geophysical Research Letters (see Exhibit A of this report), since our colleagues felt that the results are timely and important. This paper points out that Doppler shift effects in a magnetic field must be taken into account in order to convert EUV morphology into ion density distribution/morphology.

Aside from fulfilling Objectives 1 and 2 by publication of three science papers, at least five invited papers have been given, by investigators of this contract, in American Geophysical Union, International Society for Optical Engineering and COSPAR meetings, as well as numerous contributed papers. The principal investigator has chaired and organized two magnetosphere imaging special sessions for scientific society meetings. All such activities were partially under the auspices of this contract.

Objective 3: To image the magnetosphere with an EUV instrument, it is not enough to simply have an EUV normal-incidence multilayer mirror tuned to the proper wavelength. The magnetosphere is a large object, so it is necessary to demonstrate that a multilayer mirror with a wide field of view can be successfully constructed and tested. This is not a simple task because it requires proper wavelength band transmission for a highly curved surface on a mirror of large diameter. To demonstrate it is feasible, we have constructed such a mirror at 304 angstrom (the helium ion line) and demonstrated its reflectivity. The mirror constructed under auspices of this contract is indeed the world's largest 304 angstrum multilayer mirror to date. The detailed report of the construction and testing is included below as part of the main body of this report:

Fabrication and Test of a Wide Field Multilayer Mirror

The objective of the laboratory research conducted under this contract was to fabricate and test a multilayer deposited on a highly curved mirror surface. The multilayer was designed for normal incidence reflection of the emission line of He II at a wavelength of 304 A. The mirror was of a design suitable for broad field imaging of the reasonantly scattered solar He line from He+ in the earth's plasmasphere. The mirror must have a large field of view, approximately 40 deg full width, in order to effectively image large scale structures in the plasmasphere. This requires a short focal length to match available detector sizes and to minimize telescope weight and volume.

A spherical protype mirror was chosen having a radius of curvature of 9.8 cm (focal length of 4.9 cm) and a diameter of 14 cm. The sagitta for this highly curved mirror is 2.8 cm and the angle that the mirror surface makes with its axis varies from 90 deg to 45 deg, center to edge. Since the multilayer deposition rate is both a function of distance and angle of incidence, this poses a challenge to produce a multilayer that is uniform in response over the mirror's surface.

A multilayer consists of interleaved thin films of materials with differing optical constants. For normal incidence reflection of 304 A photons, molybdenum and silicon were chosen. A vacuum sputtering process, involving cylindrical planar magnetrons, is used to deposit thin films of these metals. These devices generate a magnetically confined plasma in an argon atmosphere at a pressure of ~2 mtorr. An applied electric field accelerates ionized Ar atoms which strike a target of the material to be deposited. The Ar atoms have sufficient energy to knock out, or sputter, atoms of the target material that are subsequently deposited on the multilayer substrate.

The multilayer deposition system is shown in Fig. 1. Two magnetrons, one with a Si target and the other with Mo, appear as the the cylinders that are diametrically opposed just below the disk near the top of the photograph. The deposition regions of magnetrons are bounded by the cylinders and the disk. Multilayer substrates may be mounted in holes cut in the disk, whose rotation then carries the substrate alternately over the Si and Mo deposition regions to fabricate the multilayer. Precise calibration of the deposition rates and maintaining them constant in time allows layer thicknesses to be selected and controlled throughout the multilayer. Areal uniformity of the multilayer is obtained by using appropriately shaped masks between the magnetrons and the substrate which maintain constant deposition rates over its entire area.

In order to determine the required mask shapes for deposition on the highly curved mirror, an aluminum model of the mirror was fabricated. This allowed measurements to proceed without placing the mirror at risk. Since the mirror is symmetrical, it was decided to rotate the substrate about its axis at 1 rps during the depositions. Six facets, approximately one cm square, were cut from a polished silicon wafer and mounted radially along the mirror model's surface. The model had been made with slightly larger radius of curvature to compensate for the 0.2 mm facet thickness. Thus the surfaces of the facets closely simulate the shape of the mirrors surface. As a means of calibrating the deposition rates a strip of photo-resist was applied across each facet. The faceted model was rotated over a magnetron's deposition region for a measured time interval and the photo-resist was subsequently desolved to produce a step equal in height to the amount of material deposited. Measurement of the step height and the deposition time calibrated the rate. This was done for each facet as a function of radius on the mirror model. Iteration of this

process with new facets for each trial and magnetron, while varying the shape of the mask, was carried out until satisfactorily constant step heights were obtained for all facets. The final step heights of approximately 1200 A are shown in Fig. 2. The deposition times of 1200s and 600s for the Mo and Si magnetrons have been selected to give a measurement accuracy for the step heights of approximately +- 1.5 %. The final peak to valley spread for Mo is 1.4%, while that for Si is 4.8%. Deposition rates calculated from these data are used to determine the dwell time over each magnetron that is required to fabricate the selected multilayer design.

Because of spherical aberration in a mirror with such a small focal ratio (f/0.35), only a narrow annulus of the entrance aperture can be used if acceptable angular resolution is to be obtained over a 40 deg field. While this reduces the usable effective area of the mirror, it has a beneficial effect, since baffling the mirror in this manner restricts the angle of incidence onto the mirror to a very narrow range. One may then tailor the Bragg peak of the multilayer to the average angle and the narrow angular range provides more uniform reflectivity over the field of view. A ray trace of the optics to determine this average angle of incidence was beyond the scope of this investigation. However, parameters of the present mirror are very close to those of telescopes on the ALEXIS instrument (Priedhorsky et al., 1988 and Bloch et al., 1992). In that case the average incident angle was 23 deg with a spread of ~ +- 3 deg and these parameters were used in this investigation.

The response of the selected multilayer design is shown in Fig. 3. This plot is the Bragg reflectivity of the multilayer for 304 A photons as calculated from optical constants of Mo and Si (Windt, 1989). The multilayer has a 2d-spacing of 368 A and 5 layer-pairs with Mo being 36% of the layer-pair thickness. In predicting the 2d spacing on each facet from the data of Fig. 2, a peak to valley spread of 2.9% was calculated. This is less than the percentage spread in Si step heights, since the lowest rate in Si is partially compensated by the highest rate in Mo at a radius of 1.25 cm and thus reduces the maximum spread. At the same magnetron deposition rates determined from data of Fig. 2, dwell times of 55 s over the Si magnetron and 67 s over that of Mo were determined.

Multilayers were fabricated on silicon wafer facets located, as before, at the six radii on the model mirror used for the rate calibrations. The measured 304 A reflectivity of each facet as a function of angle of incidence is shown in Fig. 4. There are clearly non uniformities from facet to facet. We attribute this to the differences in each facet's exposure as it enters and leaves the deposition region. These differences were negligable in the 600 s and 1200 s deposition times used in the rate calibrations but are apparent in the shorter exposures used in the multilayer fabrication. However, the least variation occurs near the angle of 23 deg. which is the average incident angle a telescope using this mirror would operate. Also, in a working telescope, the center of the mirror is occulted by the detector and is thus not illuminated. The variation of response is smaller if only the outer three facets are considered. Angular responses for these three facets are shown in Fig. 5 and data on average reflectivities for a +- 3 deg angular spread are given in Table I for both the full aperture and neglecting the three central facets. Maximum reflectivity variation for full aperture of +- 7 % occurs at 26 deg. For the limited aperture the maximum is +- 4 % at 20 deg with a variation of less than +- 1 % and +- 3 % at the other angles.

TABLE I: AVERAGE REFLECTIVITY +- HALF OF PEAK TO VALLEY SPREAD

	Angle (deg)		
	20	23	26
All Facets	.146+-.007	.146+-.005	.138+-.010
Outer Facets	.143+-.006	.148+-.001	.142+-.004

The data of Fig. 4 have been fitted by curves similar to Fig. 3 by varying the 2d-spacing and Mo fraction. The fits are shown in Fig. 6 and the results summarized in Table II.

TABLE II: DERIVED 2D-SPACINGS AND MO FRACTIONS FOR TEST FACETS

Radius (cm)	2d (A)	Mo Fraction
0.0	358	.36
1.25	365	.40
2.5	367	.33
3.75	371	.33
5.0	376	.32
6.25	369	.36

The data of Table II show a peak to valley spread of 5 % in 2d but 23 % in Mo fraction. This large variation in Mo fraction is much greater than expected and is not presently understood. It is unlikely that the physical thickness of Mo varies by this much and the Si layer thickness varies inversely to compensate, so the 2d-spacing (layer-pair thickness) is constant to within the observed 5 %.

The variation in reflectivity indicated in the limited aperture data of Table I is sufficiently small that it was decided to deposit a multilayer on the mirror using the same procedures as for the model and facets. This deposition was completed and a photograph of the multilayer mirror is shown in Fig. 7.

Because of the short focal length and small radius of curvature of the mirror, it is very difficult to test. A system was set up using a micro-channel plate to measure the reflectivity as a function of wavelength at a single location on the mirror. These measurements, along with similar measurements for the multilayer facet at a radius of 6.25 cm, are shown in Fig. 8. The response calculated from optical constants and the parameters of Table II for the r=6.25 cm facet is also shown by the solid line in the plot. There is reasonable agreement at the longer wavelengths but the mirror data point at 304 A and the facet point at 256 A lie off the curve outside of counting statistics, which are approximately the the size of the symbols.

In summary, we have successfully demonstrated the ability to deposit a multilayer, with uniformity better than 4 %, on highly curved mirror surfaces that are suitable for use in telescopes able to provide wide field imaging of the plasmasphere at 304 A. Utilizing a shutter to elliminate nonuniformities that occur during the interval when the mirror is being transported into and out of the deposition region will provide substantial further improvement.

REFERENCES

J.J. Bloch, W.C. Priedhorsky, D. Roussel-Dupre, B.C. Edwards and B. W. Smith, SPIE Proceedings, Conference on EUV, X-ray and Gamma-ray Instrumentation for Astronomy III, to be published, 1992.

W.C. Priedhorsky, J.J. Bloch, B.W. Smith, K. Strobel,M. Ulibarri, J. Chavez, E. Evans, O.H.W. Siegmundm H. Marshall, J. Vallerga and P. Vedder, SPIE Proceedings, 982, 188, 1988.

D. L. Windt, Appl. Opt. 30, 15, 1991.

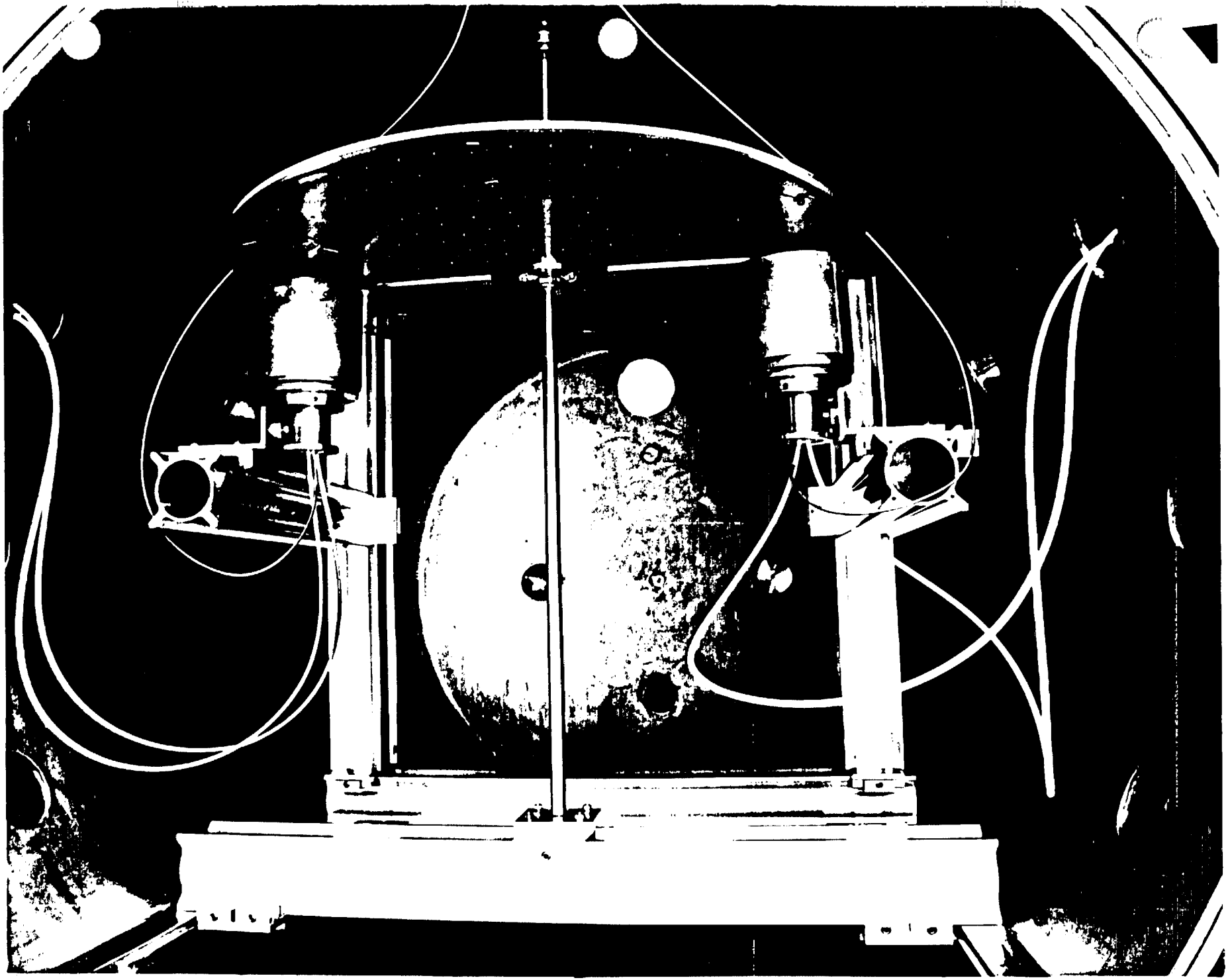

Fig. 1 Photograph of the Multilayer Deposition System.

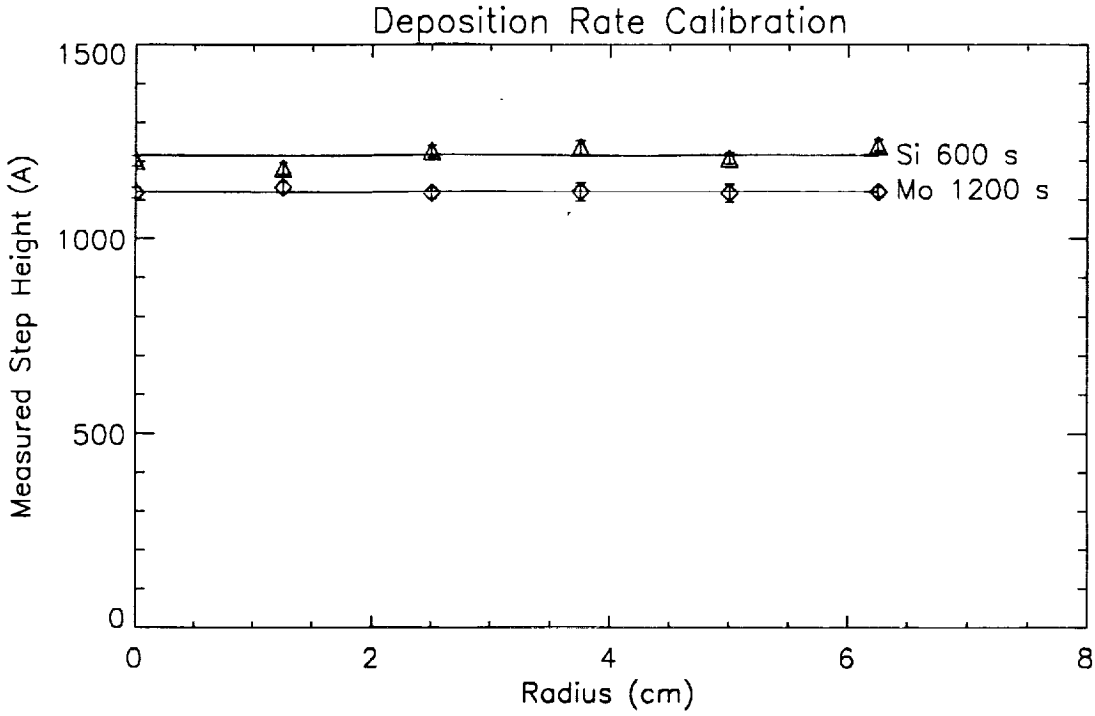

Fig. 2 Final Step Height Data for the Six Facets on the Model Mirror.

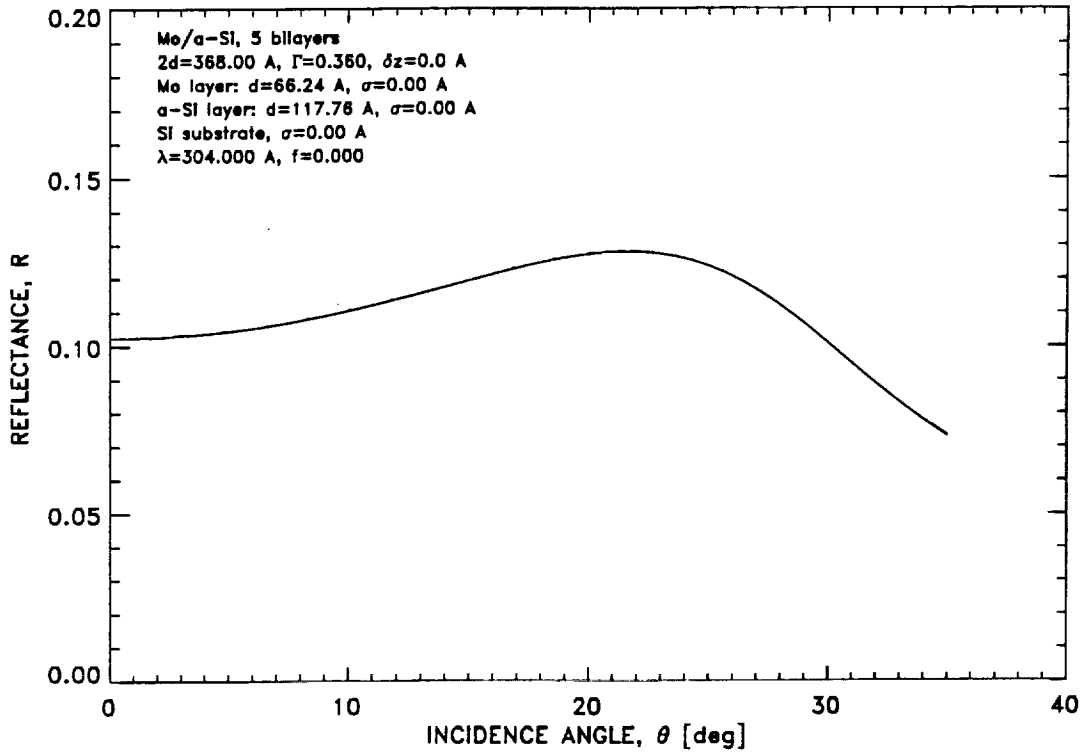

Fig. 3 Calculated Bragg Response of the Selected Multilayer Design.

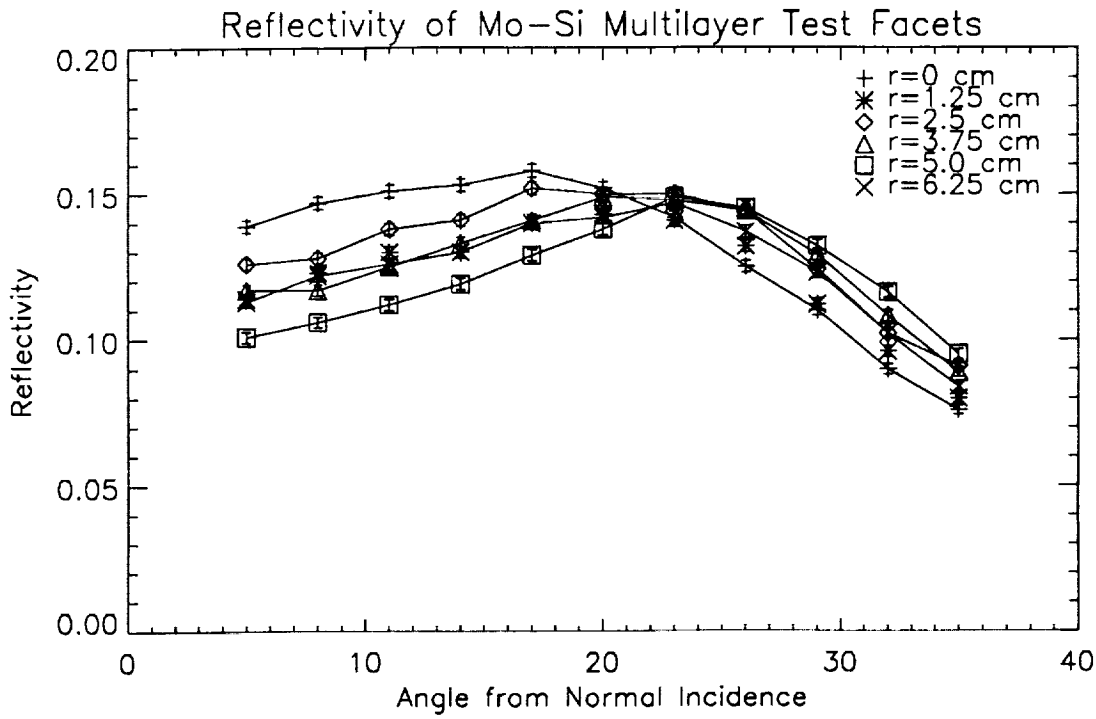

Fig. 4 Bragg Peaks for Six Facets on the Model Mirror Measured at 304 A.

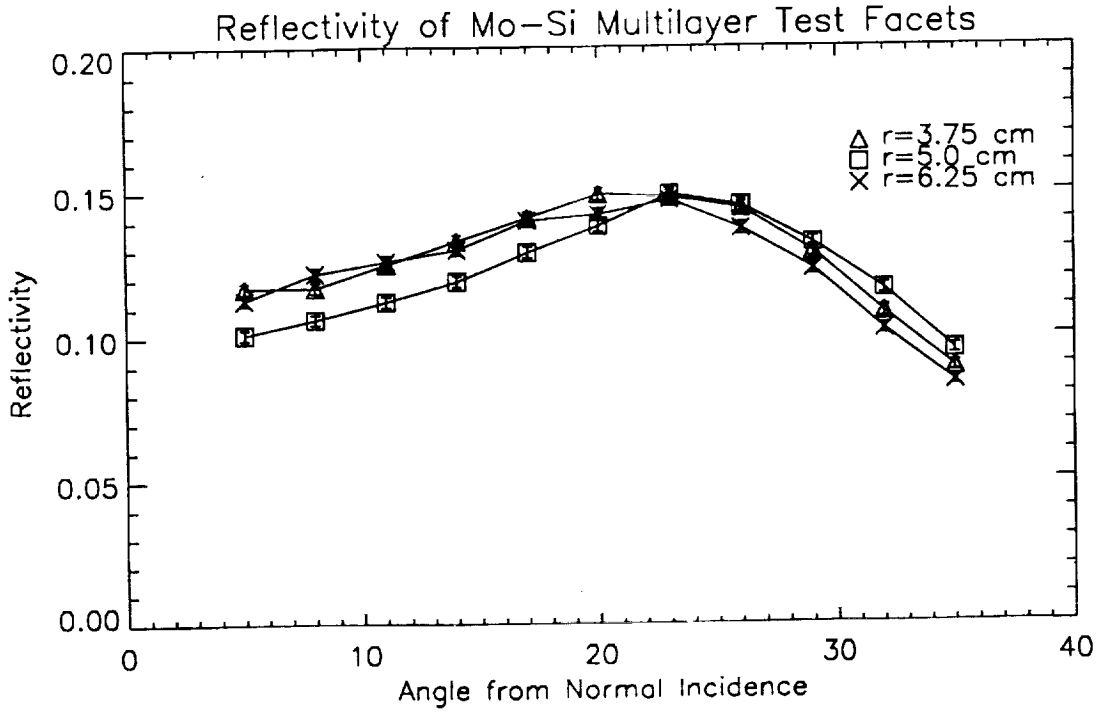

Fig. 5 Bragg Peaks for Facets on the Model Mirror Used When Properly Baffled. Measurements are at 304 A.

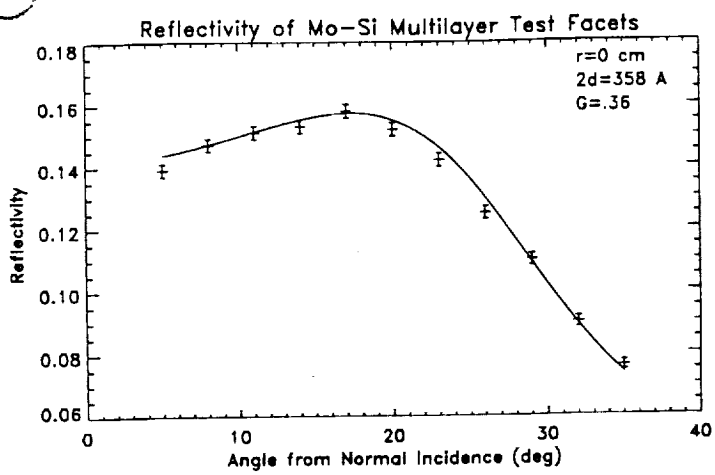

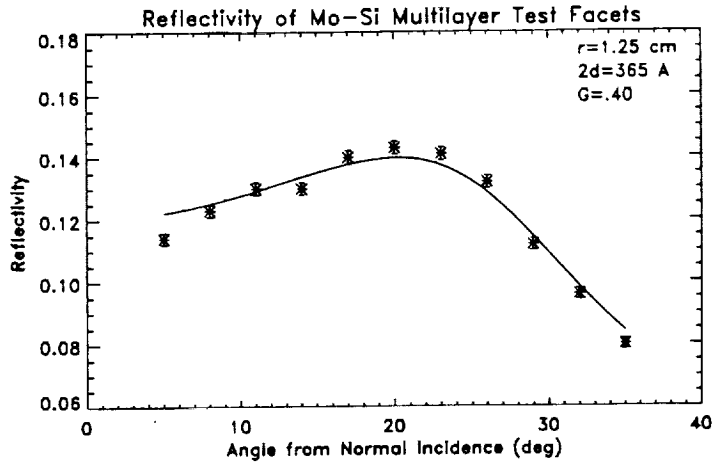

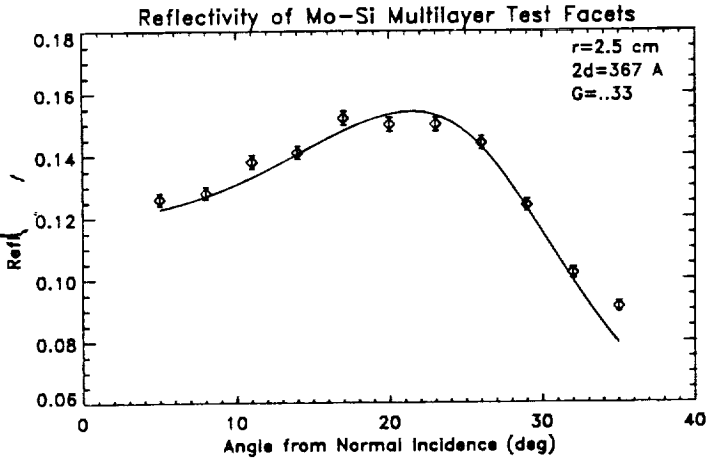

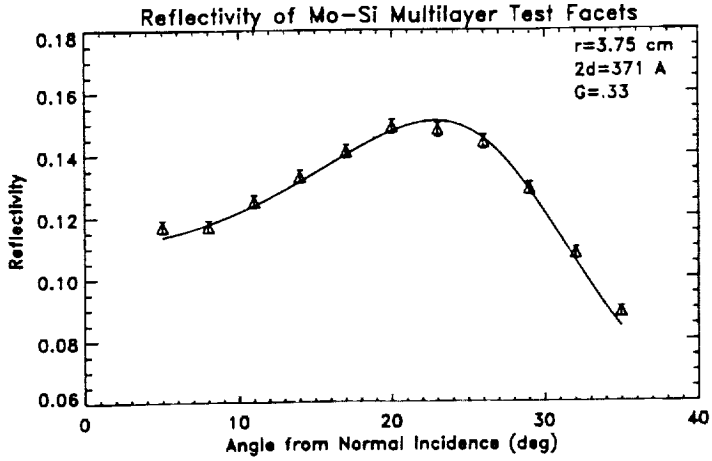

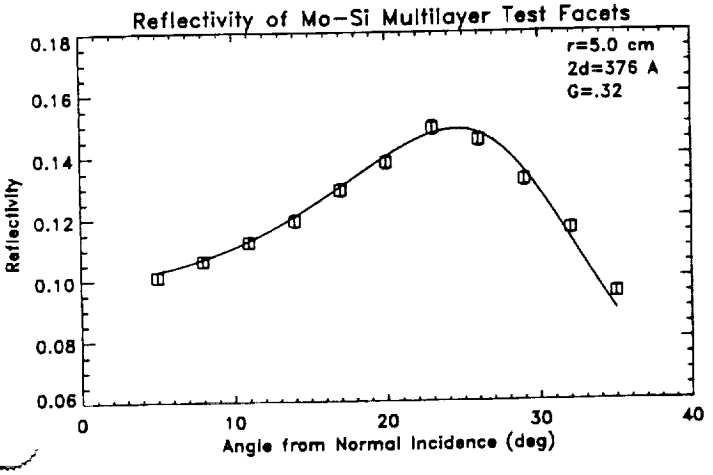

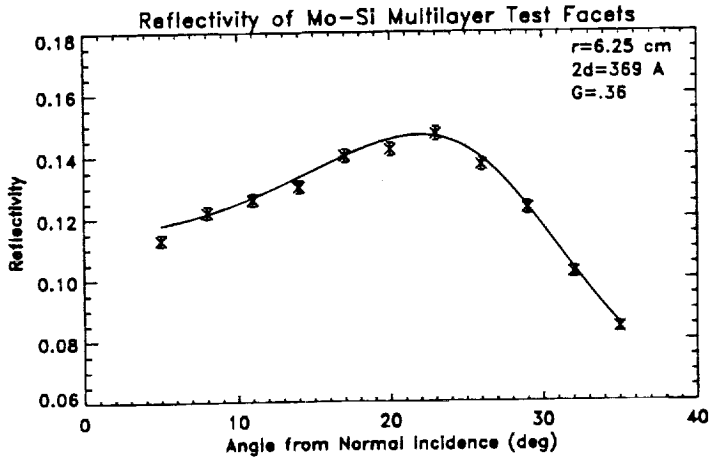

Fig. 6 Fits to the Bragg Peaks of the Six Facets.

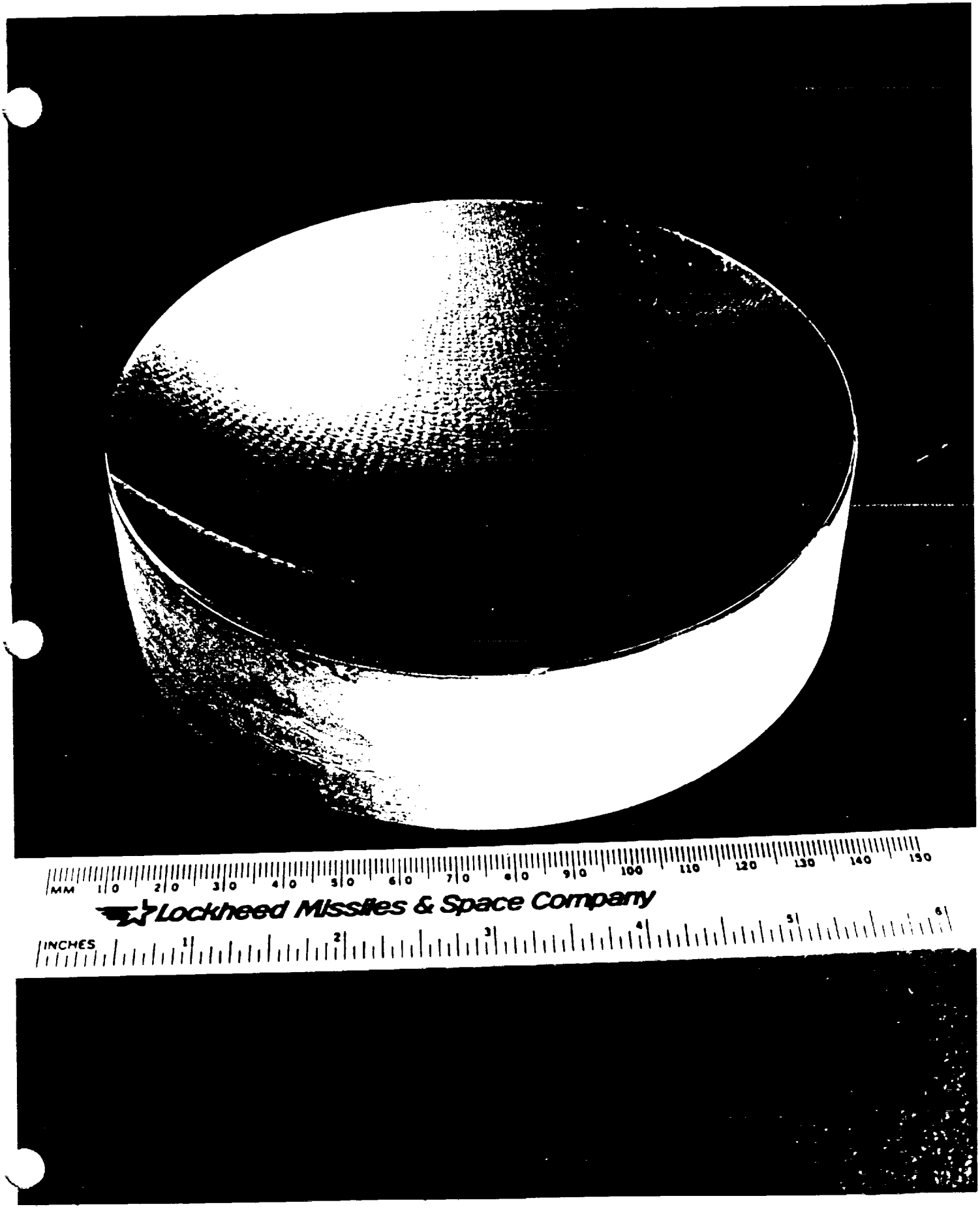

Fig. 7 Photograph of the Multilayer Mirror.

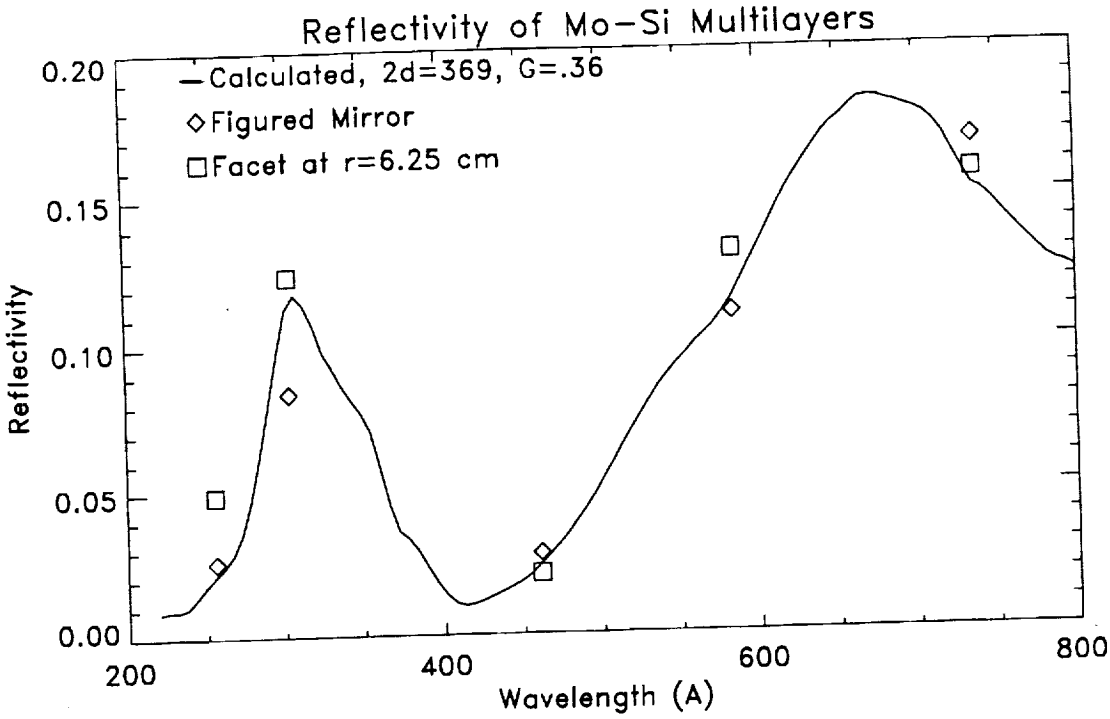

Fig. 8 Reflectivity of the Multilayer Mirror and the Facet at 6.75 cm. The Reflectivity Calculated from Optical Constants is Also Shown.

EXHIBIT A

Effects of Doppler Shifts and Source Perspectives on Extreme Ultraviolet Images of Ion Populations Moving in the Inner Magnetosphere

D. L. Murphy and Y. T. Chiu
Lockheed Palo Alto Research Laboratory, Palo Alto, California

Abstract. The full effects of solar EUV line resonant scattering by a population of ions in gyration, bounce and drift motion in the magnetosphere is formulated and demonstrated numerically with the O^+ 834 Å line as test example. It is shown that anisotropies of motion induced by the geomagnetic field and source perspective effects caused by 834 Å earthshine profoundly affect the morphology and magnitude of the EUV line images, thus enhancing the effects of Doppler shifts on narrow EUV lines. The full effects, considered for the first time here, do not impact relatively wide resonant scattering lines such as the He^+ 304 Å line.

Introduction

The scientific concept and technology of imaging inner magnetospheric ion populations in solar extreme ultraviolet resonant scattering lines have been studied extensively in the last few years [e.g., *Chakrabarti et al.*, 1982; *Chiu et al.*, 1986, 1990; *Meier*, 1990; *Swift et al.*, 1989; see also the review by *Williams et al.*, 1992 and references therein]. These independent estimates of signal intensity for some candidate resonant scattering lines were generally consistent with each other and yielded sufficient signal for morphological measurements, thus promoting the feasibility of the concept. While the above estimates are necessary to pioneer the concept, further definition of the characteristics is needed to examine how, and whether, the scientific objectives of imaging magnetospheric morphology and/or diagnostics of magnetospheric plasma processes can be achieved. This is the prime objective of this paper.

This paper reports on results of imaging simulation studies aimed at complete inclusion of Doppler shifts with respect to illumination sources for resonant scattering by an ion population executing gyration, bounce, and drift motion in the geomagnetic field. As far as we can ascertain the effects of the geomagnetic field upon the EUV images of ion populations have not been treated in full, although *Meier* [1990] and *Garrido et al.* [1991] have noted the importance of Doppler shifts on resonant scatter rates. An important result of this study is that the anisotropic control of the geomagnetic field on ion population velocity distributions significantly impacts the morphology and diagnostics of some EUV images, especially those with relatively narrow solar line widths. Further, sources of illumination strongly affect the perspective of some EUV images, because of the geomagnetic control of ion motion.

Theory

The theoretical treatment of resonant scattering is described in detail by other authors [*Mihalas*, 1978; *Meier*, 1991]. We briefly review the formalism to establish our notation. For magnetospheric ions we take the medium to be optically thin. The radiance along a line-of-sight (LOS) $\vec{r}'(s) = \vec{r} - s\hat{n}$ is

$$I(\vec{r}, \hat{n}, \nu) = \int_{LOS} ds\ \varepsilon(\vec{r}'(s), \hat{n}, \nu) \qquad (1)$$

where I is the specific intensity or radiance at observer position $\vec{r}$ for radiation of frequency ν with direction of propagation $\hat{n}$, ε is the volume emissivity for such radiation, and s is the distance along the line-of-sight of the observer. There are three main ingredients necessary for evaluating the emissivity in resonant scattering: the source intensity, the amount of scattering for an individual ion, and the ion density. For a single resonant scattering line, the emissivity is

$$\varepsilon(\vec{r}, \hat{n}, \nu) = \frac{h\nu_0}{4\pi} B_{12} \int \frac{d\Omega'}{4\pi} d\nu' d^3v\ J(\vec{r}, \vec{v}, \hat{n}, \nu, \hat{n}', \nu') \quad (2a)$$

with

$$J(\vec{r}, \vec{v}, \hat{n}, \nu, \hat{n}', \nu') = f(\vec{r}, \vec{v}) R(\hat{n}, \nu, \hat{n}', \nu', \vec{v}) I_0(\vec{r}, \hat{n}', \nu'). \qquad (2b)$$

In (2a) and (2b) $f(\vec{r}, \vec{v})$ is the phase space density of scatterers, ν_0 is the center frequency of the line, B_{12} is the Einstein absorption coefficient, R is the Hummer redistribution function, normalized so that

$$\int \frac{d\Omega}{4\pi} d\nu \frac{d\Omega'}{4\pi} d\nu' R = 1, \qquad (3)$$

and I_0 is the incident intensity.

The formalism in this paper is applicable to any resonant scattering line, such as the helium 304 Å line and the oxygen 834 Å lines. Our results show that motion in the geomagnetic field does not affect the apparent morphology of 304 Å images unless the helium ions are very hot, because of the large solar line width; whereas it profoundly affects the oxygen 834 Å images. Therefore, we formulate here the more complex oxygen problem in some detail.

The solar 834 Å complex comprises 9 spectral lines, a mixture of O^+ and O^{++} emissions. We associate the values of the index j from 1 to 3 with the three O^+ lines, and let values of j ranging from 4 to 9 correspond to the six O^{++} emissions. *Meier* [1990] has tabulated the statistical weights with which these lines appear in the solar 834 Å blend. We use the notation ν_{0j} to denote the center frequency of the j^{th} line, and $\Delta\nu_j$ to denote its width. We also denote by p_j the probability that a solar photon in the 834 Å line complex was emitted *via* the j^{th} transition.

The source intensity is the sum over the three solar O^+ lines, the six solar O^{++} lines, and the three earthshine O^+ lines. We first consider the solar emissions; we will discuss earthshine emissions below. For the solar lines we have

$$I_0 = \sqrt{\pi}\ h\nu\ F_0\ \delta(\hat{n}\cdot\hat{k}-1)\ \sum_j \frac{p_j}{\Delta\nu_j} e^{-[(\nu-\nu_{0j})/\Delta\nu_j]^2}. \quad (4)$$

In this expression, $\hat{k}$ is the direction of propagation of a solar photon and $F_0 = 6.7 \times 10^8$ photons/cm^2/sec is the solar 834 Å flux [*Hinteregger et al.*, 1981]. We ignore the finite angular size of the sun.

Following *Meier* [1991], Hummer's redistribution function for the k^{th} magnetospheric O^+ line is given by

$$R_k = \delta[\nu' - \nu_{0k}(1+\frac{\vec{v}\cdot\hat{n}'}{c})]\ \delta[\nu'-\nu+\nu_{0k}\frac{\vec{v}\cdot(\hat{n}-\hat{n}')}{c}] \quad (5)$$

if we assume an isotropic phase function. We will take the sum over the three O^+ 834 Å lines below. The incident radiation is described by frequency ν' and direction of propagation $\hat{n}'$, the scattered radiation is described by the corresponding unprimed variables.

The phase space density for magnetospheric O^+ is taken to be Maxwellian at an altitude of 1000 km, for all invariant latitudes and magnetic local times. The model of *Tsyganenko* [1987] defines the magnetic field. We use conservation of energy and first adiabatic invariant to map this distribution up magnetic field lines to other points in the magnetosphere; these two conservation laws will also provide the boundaries of integration in velocity space. For magnetospheric ion populations, the temperatures parallel and perpendicular to the magnetic field are generally not equal and the general formalism of *Chiu and Schulz* [1978] applies. If $T_\parallel$ and $T_\perp$ are not equal, the resonant scattering Doppler shift effects are more severely anisotropic with respect to the magnetic field direction. For the present work, we shall, for the sake of brevity of expressions, assume $T_\parallel = T_\perp$, which has the least anisotropy; we denote the common temperature by T. Thus,

$$f = n_0\left[\frac{m}{2\pi kT}\right]^{3/2} \exp[-\frac{m}{2kT}(v^2 - v_0^2)] \quad (6)$$

where m is the mass of an O^+ ion, $r_0 = |\vec{r}_0| = 1.157R_E$, and v_0^2 is given by

$$v_0^2 = 2GM_E\left(\frac{1}{r}-\frac{1}{r_0}\right) - \frac{2e}{m}[\phi(\vec{r})-\phi(\vec{r}_0)] \quad (7)$$

In (7) $\vec{r}_0$ denotes the intercept of the magnetic field line with 1000 km altitude and ϕ is the magnetospheric electric potential. Although ϕ is not utilized in the present work, which deals with a trapped O^+ ion population, we plan to use this capability in the future to incorporate the effects of

parallel electric fields upon ion outflows. The boundaries of integration in velocity space are given by $v^2 \geq v_0^2$ and $v^2|\vec{B}(\vec{r}_0)|\sin^2\alpha \leq [v^2 - v_0^2]|\vec{B}(\vec{r})|$, where α is the pitch angle, i.e., $\cos\alpha = \vec{v}\cdot\vec{B}/(|\vec{r}||\vec{B}|)$.

With all ingredients at hand from (4), (5), and (6), the scattered intensity at the detector is given by substitution of (2a-b) into (1). The intensity function $I(\vec{r},\hat{n},\nu)$ is usually integrated over the instrument band pass. In this paper, we are not concerned with instrument effects; therefore, we integrate over the entire band assuming that there are no other background lines.

The result for the total radiance, including the sums over spectral lines, is

$$\int I\,d\nu = \frac{F_0 h^2}{16\pi^{3/2}} \sum_{j,k} \frac{p_j}{\Delta\nu_j} \nu_{0k}^2 B_{12k} \int ds\, d^3v\, f\,(1 + \frac{\vec{v}\cdot\hat{k}}{c}) \exp[-X] \qquad (8a)$$

where

$$X = \left[\left(\nu_{0k}(1 + \frac{\vec{v}\cdot\hat{k}}{c}) - \nu_{0j}\right)/\Delta\nu_j\right]^2. \qquad (8b)$$

Upon substitution for f, the integral over velocities becomes, up to a constant of proportionality,

$$\int d^3v\ (1 + \frac{\vec{v}\cdot\hat{k}}{c})\ \exp[-A], \qquad (9)$$

with

$$A = \frac{m}{2kT}[v^2 - v_0^2] + X \qquad (10).$$

Using spherical coordinates v, α, and β in velocity space, the velocity space integration boundaries cited above can be expressed as step functions

$$\Theta[v^2 - v_0^2]\,\Theta[(v^2 - v_0^2)B - v^2 B_0 \sin^2\alpha] \qquad (11)$$

with $B = |\vec{B}(\vec{r})|$ and $B_0 = |\vec{B}(\vec{r}_0)|$. The velocity space coordinate axes depend upon the direction of the magnetic field $\vec{B}(\vec{r})$. It is now clear that the integrated scattered intensity $\int I\,d\nu$ depends on direction with respect to the magnetic field upon velocity space integration.

We include earthshine effects by assuming that above 1000 km the illuminated hemisphere of the earth is a Lambertian radiator of O^+ 834 Å emissions with a brightness of 1.5 kilorayleigh. Note that we do not address the problem of the optically thick upper atmosphere, but only include its emissions as the earthshine source intensity illuminating the magnetosphere above 1000 km altitude. The radiating atmospheric ions are assumed to have a thermal velocity distribution with a temperature of 1000 K. This reduces the width from the solar width by the square root of the ratio of the upper atmospheric temperature to the

solar atmospheric temperature. An additional complication is the integration over the solid angle subtended by the illuminated earth, since the earthshine source intensity is a non-trivial function of the position along the line of sight and the photon direction of propagation. Thus, the evaluation of resonantly scattered earthshine radiance involves a six dimensional integration—the line of sight, the three dimensional velocity space, and the two angular coordinates for the visible illuminated earth—whereas the resonantly scattered solar radiance is given by a four dimensional integration.

Discussion and Conclusions

We have evaluated these radiance integrals through Monte Carlo integration. In this integration method, the integrand is factored into two pieces. One piece is a probability density function defined on the volume of integration, e.g., the three-dimensional velocity space and the one-dimensional line-of-sight, for the case of solar illumination. The other piece then becomes a function of random variables defined on the volume of integration, so that the original integral is now to be interpreted as the expectation value of this function. In Monte Carlo integration, a series of statistically independent points in the volume of integration is chosen at random according to the aforementioned probability density function. The function whose expectation value is to be determined is evaluated at each of these chosen points, and this ensemble of function values, when averaged, provides an estimate for the expectation value. By carrying out this process several times, an estimate for the uncertainty in the evaluation of the integral can also be obtained. For more information on Monte Carlo integration, see *Press et al.* [1986] and references cited therein.

We assumed a 10 eV oxygen ion reservoir at 1.157 R_E, with a spatial density of 100 O^+ ions per cm^3. The images shown are 31 × 31 pixels, smoothed to 60 × 80 pixels by linear interpolation. Statistical errors in the evaluation of the O^+ column density are about 1% or less for each pixel; statistical errors in the evaluated radiance range from 3% to 10%, with a typical value of 4%. We believe these errors to be uncorrelated from one pixel to another (prior to smoothing). With this integration code, we have simulated views in the magnetospheric 834 Å band from 9 R_E out for three spacecraft perspectives: tailward, dawnward, and toward the direction of the negative z-axis (in solar-ecliptic coordinates). Hereafter these will be referred to as "images" for brevity.

As has been pointed out by *Meier* [1990] and *Garrido et al.* [1991], Doppler effects are important for O^+ 834 Å scattering in the magnetosphere. They appear in the resonant scattering formalism through the $\vec{v} \cdot \hat{n}$ and $\vec{v} \cdot \hat{n}'$ terms in the Hummer redistribution function. In order to highlight the effects of the Doppler shift, we compare the

full effects images with images produced with those terms set to zero. The image in Fig. 1a is a dawnward view, from 9 R_E, with all effects (Doppler shift, geomagnetic field, and earthshine) accounted for. Fig. 1b shows the *difference* between an image including all effects except for Doppler effects, and the image in Fig. 1a. This difference is itself several times brighter than the full effects image, out to a few R_E on the dayside. On each of these images, as well as on the images described below, we have marked on an outline of the earth the location of the magnetic north pole.

We determine the importance of geomagnetic field effects on magnetospheric images in EUV by evaluating the radiance integrals without the limitations set by geomagnetically trapped motion. The result of the angular integration in velocity space is then scaled to give the same spatial density of O^+ ions, at each point along the line of sight, as would be obtained with the velocity space boundaries present. Thus, all pitch angles are available to the scattering O^+ ions, unlike the geomagnetically trapped population. To our knowledge, the evaluation of the influence of geomagnetic effects on EUV images has not heretofore been carried out. The basic cause of the geomagnetic effects is the anisotropy induced by the geomagnetic field on the parallel and perpendicular velocity distributions of a trapped population executing gyration and bounce motion. With all pitch angles available, the expected radiance is enhanced in the auroral regions and reduced in the equatorial regions. Unless the importance of geomagnetic field effects on O^+ ion pitch angle distributions is recognized, misinterpretation of such magnetospheric EUV images will result. Figs. 2a and 2b display the differences in morphology due to the inclusion/omission of pitch angle effects. Fig. 2a is an image of the difference: [all effects] - [all effects but for pitch angle effects]; Fig. 2b displays the difference: [all effects but for pitch angle effects] - [all effects]. In both images, values of the radiance difference less than 10^{-3} Rayleigh are set to white. Comparing these difference images with the full image Fig. 1a, we see that (1) the magnitude of the difference is a substantial part of the full image at the important altitudes $> 1R_E$, and (2) the difference images in Fig. 2b have the morphology of magnetic field lobes, showing the important combined influences of Doppler shifts and geomagnetic field on imaging the morphology of the O^+ population.

Earthshine is an important source of 834 Å illumination out to a couple R_E on the dayside, as shown by Fig. 3b, which is to be compared to Fig. 3a. Each of these images is a view looking toward the negative solar-ecliptic z axis from a distance of 9 R_E. Fig. 3a includes all effects, whereas Fig. 3b omits the effects of earthshine and includes only Doppler and geomagnetic effects. The relative importance of solar and terrestrial sources of EUV depends upon

solar and magnetospheric activity and atmospheric conditions. Comparison of Figs. 3a and 3b shows that, whereas the morphologies of the two are similar, the Doppler and geomagnetic effects combined with earthshine effects profoundly influence the expected image intensity, thus impacting the proper interpretation in terms of plasma diagnostics.

Acknowledgment. This paper is supported by NASA contract NASW-4529, and by the Lockheed Independent Research Program.

References

Chakrabarti, S., F. Paresce, S. Bowyer, Y. T. Chiu, and A. Aikin, Plasmaspheric helium ion distribution from satellite observations of He II 304-Å, *Geophys. Res. Lett., 9,* 151, 1982.

Chiu, Y. T., R. M. Robinson, G. R. Swenson, S. Chakrabarti, and D. S. Evans, Imaging the outflow of ionospheric ions into the magnetosphere, *Nature, 322,* 441, 1986.

Chiu, Y. T., and M. Schulz, Self-consistent particle and parallel electrostatic field distributions in the magnetospheric-ionospheric auroral region, *J. Geophys. Res., 83,* 629, 1978.

Chiu, Y. T., R. M. Robinson, H. L. Collin, S. Chakrabarti, and G. R. Gladstone, Magnetospheric and exospheric imaging in the extreme ultraviolet, *Geophys. Res. Lett., 17,* 267, 1990.

Garrido, D. E., R. W. Smith, D. S. Swift, and S.-I. Akasofu, Imaging the Earth's magnetosphere: effects of plasma flow and temperature, *Planet. Space Sci., 39,* 1559, 1991.

Hinteregger, H. E., K. Fukui, and B. R. Gilson, Observational, reference, and model data on solar EUV, from measurements on AE-E, *Geophys. Res. Lett., 8,* 1147, 1981.

Meier, R. R., The scattering rate of solar 834 Å radiation by magnetospheric O^+ and O^{++}, *Geophys. Res. Lett., 17,* 1613, 1990.

Meier, R. R., Ultraviolet spectroscopy and remote sensing of the upper atmosphere, *Space Sci. Rev., 59,* 1, 1991.

Mihalas, D., *Stellar Atmospheres,* W. H. Freeman and Co., San Francisco, 1978.

Press, W. H., B. P. Flannery, S. A. Teukolsky, and W. T. Vetterling, *Numerical Recipes, the Art of Scientific Computing,* Cambridge University Press, 1986.

Swift, D. W., R. W. Smith, and S.-I. Akasofu, Imaging the Earth's magnetosphere, *Planet. Space Sci., 37,* 379, 1989.

Tsyganenko, N. A., Global quantitative models of the geomagnetic field in the cislunar magnetosphere for different disturbance levels, *Planet. Space Sci.*, *35*, 1347, 1987.

Williams, D. J., E. C. Roelof, and D. G. Mitchell, Global magnetospheric imaging, *Rev. Geophys.*, *30*, 183, 1992.

Figure Captions

Fig. 1: (a) Simulated magnetospheric 854 Å image from 9 R_E above the dusk meridian, looking dawnward, including effects of Doppler shifts, velocity space anisotropies due to the geomagnetic field, and earthshine; (b) same perspective as in (a), but now the image shown is the difference between an image omitting Doppler effects and the image in (a).

Fig. 2: Views displaying the difference between a simulated image including all effects, and one omitting geomagnetic pitch angle effects, for the perspective of Fig. 1. (a) [all effects included] - [geomagnetic effects omitted]; (b) [geomagnetic effects omitted] - [all effects included].

Fig. 3: Simulated magnetospheric images looking down from the positive solar-ecliptic z-axis to show the effects of earthshine. (a) is an image with all effects included; in (b), the effects of earthshine have been omitted.

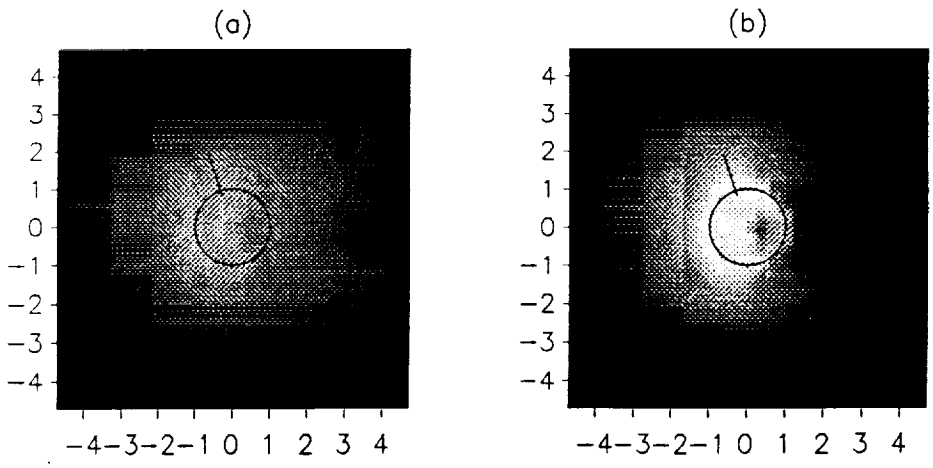

Figure 1

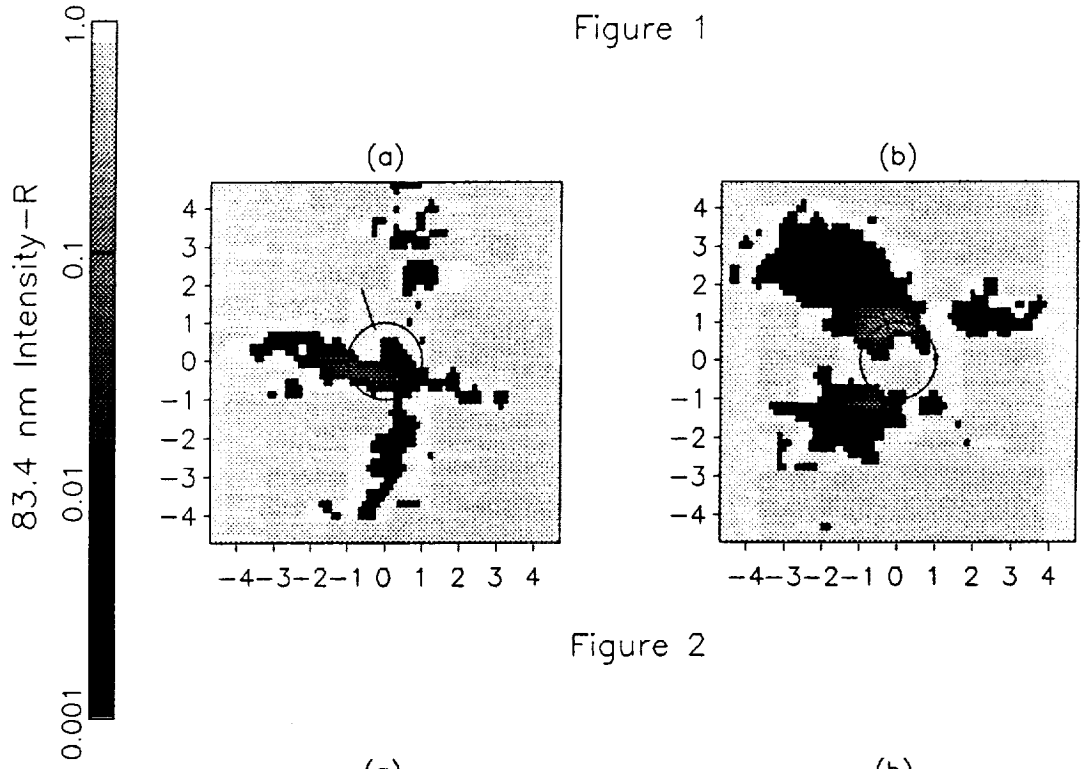

Figure 2

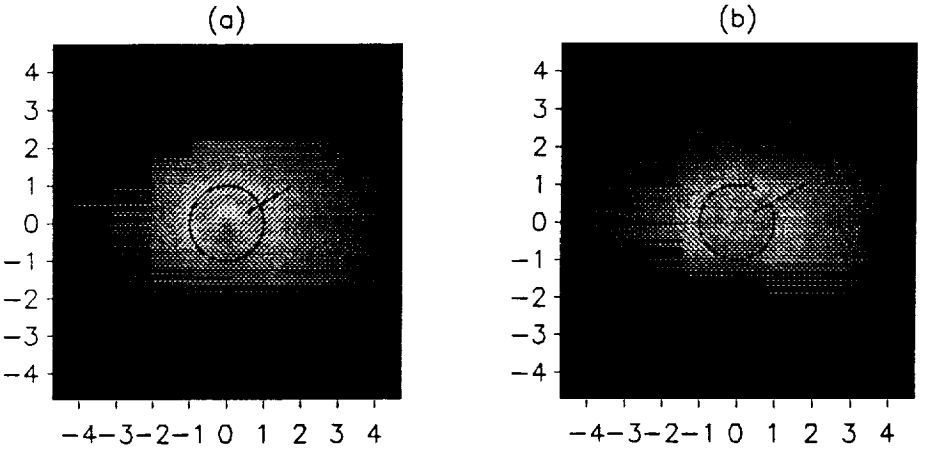

Figure 3

EXHIBIT B

Magnetospheric Imaging of High Latitude Ion Outflows

D.E. GARRIDO[1], R.M. ROBINSON, Y.T. CHIU, H.L. COLLIN

Lockheed Palo Alto Research Laboratory, 3251 Hanover St., Palo Alto, CA., 94304, U.S.A.

R.W. SMITH AND D.W. SWIFT

Geophysical Institute and Department of Physics, University of Alaska-Fairbanks, Fairbanks, AK. 99775-0800, U.S.A.

Simulation of magnetospheric emissions from resonant scattering of sunlight by upward flowing He^+ (30.4 nm) and O^+ (83.4 nm) ions at high latitudes have been constructed for different satellite viewing locations and distances from the earth. The ion outflow data obtained by the Lockheed Ion Mass Spectrometer (EICS) on board the DE-1 spacecraft has been used to take into account the non-uniform distribution of ion flux intensities. For a polar orbiting satellite we obtain emission rates from outflowing ions of 5.2×10^{-2} and 5.6×10^{-2} Rayleighs for quiet and disturbed times for He^+ and 6.5×10^{-2} and 7.5×10^{-2} Rayleighs for quiet and disturbed times for O^+, respectively. These low light levels are due to use of ion outflow data only. Emission levels from all ions can be quite a bit higher and awaits further data reduction from the Lockheed instrument. We find that viewing at a distance of 9 R_E with an instrument field of view of at least 30 degrees that includes an occultation disk in the image is sufficient to exclude the bright emissions coming from plasmaspheric He^+ ions. Because the O^+ intensities increase dramatically with magnetic activity, they represent a good signature of substorm-related processes. In our modeling we assume that the ions move along dipole magnetic field lines with a density profile that is modeled by a simple magnetic field scaling. The Doppler shift of these moving ions modify the intensity of the resonantly scattered emissions. For He^+ the Doppler effects tend to decrease the intensities of the magnetospheric images while for O^+ at sufficiently high velocities the intensities may increase because enhanced scattering occurs.

1. INTRODUCTION

Interest in global imaging of the magnetosphere in the ultraviolet has been initiated by Swift et al. (1989), Chiu et al. (1990), Meier (1991) and Garrido et al. (1991). Swift et al. (1989) constructed images of the plasmasheet and ring currents from resonantly scattered light from O^+ ions. Chiu et al. (1990) simulated images of outflowing O^+ (83.4 nm) ions and neutral O (130.4 nm) atoms by considering a geostationary satellite viewing at a distance of 6 R_E in the dusk meridian. They assumed particle motions along a static dipole field with tilt and a density profile that is modeled by a simple magnetic field scaling. A uniform flux distribution over the polar region was assumed with a value derived by averaging outflowing ion fluxes measured by the EICS instrument on DE-1. The resulting column emission rates ranged between .01-1 Rayleighs. Effects of gyromotion of the ions and Doppler shifting due to the ions bulk velocity along the sun-earth direction was not considered. The calculations of Chiu et al. (1990) also did not include the bright resonant emissions originating from the plasmasphere which can obscure those emissions coming from the high latitude ion fluxes.

Meier (1991) provided a detailed assessment on the possibilities of remote sensing in the ultraviolet over a broad range of wavelengths that includes the 30.4 and 83.4 nm resonant lines of He^+ and O^+, respectively. Using plasmaspheric models based on the observations of Meier and Weller (1972) and Weller and Meier (1974), images of the plasmasphere were constructed at a viewing distance of 10 R_E in the dawn to dusk meridian plane and at various satellite locations defined by geographic latitudes 0, 30, 60 and 90 degrees. The extent of the plasmapause boundary is visible

APPENDIX 1

IMAGING THE MAGNETOSPHERE IN THE EXTREME ULTRAVIOLET

Annual Progress Report
NASA Contract NASW 4529
Code SS, NASA Headquarters
Washington, D.C. 20546

Date: **December 17, 1991**

Principal Investigator:
Dr. Y.T. Chiu, (415) 424-3421

Lockheed Palo Alto Research Laboratory
Space Sciences Laboratory, Department 91-20, B255
3251 Hanover Street, Palo Alto, CA 94304

A. PROGRESS

This report summarizes work performed to date on NASW-4529: Imaging the Magnetosphere in the Extreme Ultraviolet. In the ten month's elapse time, contract activity was focused on three tasks scheduled to proceed more or less in parallel. These are:

(1) Establishment of reliable estimates of expected solar EUV resonance scattering fluxes at He^+ 304Å and O^+834Å lines based on He^+ and O^+ fluxes measured by Lockheed's ion mass spectrometer (EICS) on board the NASA Dynamics Explorer satellite.

Mr. Harry Collin, ion mass spectrometer data scientist in our laboratory, participated in this data reduction, effort as did Mr. Dante Garrido, graduate student from the University of Alaska Fairbanks working on magnetosphere imaging as thesis topic. Under agreement by the P.I. and Dr. Akasofu of UAF, Mr. Garrido was sponsored by Lockheed via UAF's NASA Space Grant program for which Lockheed agreed to provide salary support to Mr. Garrido to participate in the data analysis and the computer image simulation efforts. Because this data analysis effort requires more resources than is allocated in NASW-4529, part of the data analysis effort is funded by Lockheed's independent research program. This collaborative effort proves to be fruitful as Mr. Garrido's work at Lockheed will constitute the major part of his Ph.D. thesis and it leads to a publication.

Two publications resulted from our effort to simulate magnetosphere EUV imaging based on in situ ion mass spectrometer data. The concept is to map all relevant in situ ion mass spectrometer data along magnetic field lines to an altitude of 1000 km in order to build up a statistical global distribution of ions on the 1000 km surface. Then the statistical fluxes distribution is treated as an instantaneous ion flux distribution, which we map up the field line as a surrogate magnetospheric ion population. Computer simulation of a magnetosphere image then proceeds by allowing the ions to resonantly scatter solar EUV lines into an imager of given optical characteristics. The results are summarized in the abstracts of the two publications whose front pages are attached to this report as Exhibits 1 and 2. Exhibit 1 is published in the Geophysical Research Letters and Exhibit 2 is to be published in Planetary and Space Science, in deference to our UAF colleagues' preference.

(2) Multilayer mirror design for a wide field-of-view 304Å imaging telescope.

For space-based imaging the magnetosphere in the next decade, our examinations, with computer simulations such as those in Exhibits 1 and 2, indicate that the only viable technique is that of multilayer mirror normal incidence imaging in the He^+ 304Å line. No 834Å multilayer mirror has been manufactured or flown to date. The first and only 304Å mirror has been flown by a Lockheed-Stanford collaboration for astrophysical objects imaging, although such imaging requires relatively small field-of-view. For wide field-of-view imagery required for magnetosphere imaging, multilayer mirror design has to be considered afresh. Dr. Dick Catura of our laboratory is the leader of this multilayer mirror design and manufacture effort for the astrophysical collaboration.

Dr. Catura was asked to consider design of an imaging mirror at 304Å with large field of view. Exhibit 3, the front page of a paper by Dr. Catura, illustrates the capability and facility of our laboratory on multilayer mirror design and manufacture.

A molybdenum-silicon multilayer mirror suitable for 304Å magnetosphere imaging has been designed with good angular response of ±10 degrees. Exhibit 4 shows the reflectance curve of the designed multilayer with a sharp peak of about 15% at 300Å . Filters are usually required to cut out unwanted reflectance at both long and short ends of the

spectrum. Such filters can be designed as multilayers also. Exhibits 5 and 6 show the angular response of the multilayer for two options of slightly different multilayer parameters. The important point for magnetospheric imaging is that a wide field of view mirror is possible.

(3) Extraction of physical parameters from images.

For magnetospheric imaging to be a science project of sufficient value, it is necessary to go beyond the mere making of a magnetospheric image. Consequently, we devote a small portion of our resources this year to investigate the theoretical possibility of extracting information from the images. Among these, we have chosen to investigate the possibility of extracting ion temperature and/or ion outflow information in the inner magnetosphere. Further, to make reliable images, the Doppler shift of moving magnetospheric ions relative to the resonant scattering line frequencies must be investigated. This important point has recently been pointed out by our collaborator, Dr. Bob Meier of NRL, and a linear motion treatment was given by Dr. Meier for the case of the O^+834Å line (Exhibit 7) . However, for a hot ion population gyrating and outflowing along a magnetic flux tube, the Doppler shift is not so simply accounted for. As a result, we initiated a proper calculation of 304Å and 834Å resonance scattering by He^+ and O^+ ions with proper magnetospheric characteristics. The calculation is quite complex, as can be seen from Exhibit 8, which summarizes its basic ingredients.

B. FUTURE WORK

For continuation in 1992 of the current project, we intend to proceed with the second phase of all three tasks whose progress in 1991 are summarized above.

(1) Imaging simulation with Lockheed data.

For this task, the 1992 emphasis will be to push the consideration of our publication (Exhibit 2) towards lower latitudes. This will be consonant with objectives of NASA's Inner Magnetosphere Imager mission. The state of data processing for Lockheed's EICS instrument for lower latitudes is not as advanced as for higher latitudes. However, we estimate that sufficient resources will be available to complete this task in CY 1992-1993.

(2) Multilayer mirror design for 304Å imaging.

The optical properties of our mirror designed will further be defined with computer simulations. A small mirror will likely be available from our parallel Lockheed independent research project which is not confined to space-based imaging. We intend to perform vacuum exposure and long-term outgassing experiments on this mirror in order to determine its performance in the space environment. Finally, if resources are available we intend to revisit the critical issue of mirror uniformity because it is critical to the upgrade from small field-of-view astrophysical imaging applications to wide field-of-view magnetospheric imaging applications.

(3) Image Exploitation

We shall complete the formulation of the Dopper shift problem outlined in Exhibit 8 of the PROGRESS section. A computer simulation of the problem outlined in Exhibit 8 will be completed in CY 1992.

EXHIBIT 1

GEOPHYSICAL RESEARCH LETTERS, VOL. 17, NO. 3, PAGES 267-270, MARCH 1990

MAGNETOSPHERIC AND EXOSPHERIC IMAGING IN THE EXTREME ULTRAVIOLET

Y. T. Chiu, R. M. Robinson, H. L. Collin

Lockheed Palo Alto Research Laboratory, Palo Alto, California

S. Chakrabarti, G. R. Gladstone

Space Sciences Laboratory, University of California, Berkeley

Abstract. Extreme ultraviolet line emissions by exospheric oxygen ions and neutrals of ionospheric origin can be used to form images of the dynamic magnetospheric regions with sufficient speed to provide a new global means of observing the dynamics of magnetosphere-ionosphere coupling processes. Computer simulations of such exospheric images based on the latest measurements of ion outflow, on known or estimated solar fluxes, and on known emission and excitation rates are shown. An evaluation of the current and foreseeable EUV imaging technology relevant to magnetospheric imaging is also given.

Introduction

The idea of using photometric or imaging techniques on ionic emission lines to obtain images or density distributions of magnetospheric and exospheric regions of the Earth began with observations of far ultraviolet emissions from neutral hydrogen and ionized helium reported by Young et al. [1971] and Johnson et al. [1971]. Chakrabarti et al. [1982] used solar resonance scattered emissions from HeII at 304Åto map the helium distribution in the plasmasphere. The full concept of EUV exospheric imaging with a set of EUV lines was discussed together with a search for possible verifications from some existing photometric data by Chiu et al., [1986]; instrument concepts were also discussed [Chakrabarti et al., 1986]. These studies indicated that exospheric imaging was technologically feasible in the inner magnetosphere ($\leq$10 R_E) with what was known about emission sources and instrument capabilities at the time. Recently, there has been a resurgent interest in EUV magnetospheric imaging at greater distances using observations from a lunar base [Swift et al., 1989].

The purpose of this paper is to re-examine the exospheric imaging concept in the light of three important new developments: (1) new information about the outflow of ionospheric ions, (2) recent calculations of the escape fluxes of neutral O^0 and H^0 due to charge exchange, and (3) the development of layered synthetic microstructure (LSM or multilayer) sensors which will result in drastic reductions in the size, increases in the speed, and enhancements in imaging quality of EUV instruments.

Magnetospheric and Exospheric Imaging

Magnetospheric imaging requires the observation of emissions of ionized constituents because the distribution of these particles is constrained by the magnetic field. During quiet times H^+ is the dominant ion in the magnetosphere, but H^+ emissions cannot be detected optically. He^+ is also a candidate for use in magnetospheric imaging but there is not enough He^+ in the outer magnetosphere to image the regions of interest. O^+ of ionospheric origin can have sufficient concentration in the magnetosphere for use in imaging. Also, escaping O^+ charge exchanges and produces O^0 which can be imaged. Although the 1304Å triplet is optically thick in the lower thermosphere, at altitudes above ~1000 km it is optically thin. Since the ground state sub-levels of the exospheric O^0 are not expected to be in thermal equilibrium, only the 1302Å component has been used in calculating the g-factor for this feature.

The EUV line emissions that we shall consider for imaging are produced by resonance scattering of solar light by the relevant constituents. In the following, simulations and observational techniques for EUV images of O^+ and O^0 will be discussed as an example of the key elements of magnetospheric imaging. Lack of space precludes discussion of other emission lines.

The brightness, $4\pi I$, of an optically-thin emission line excited by solar scattering is given by

$$4\pi I = g \int N(\ell)\, d\ell \qquad (1)$$

where $\int N\, d\ell$ is the column density of atoms/ions along the line of sight ℓ and the g-factor is estimated by

$$\begin{aligned} g &= \pi^{1/2}\, \sigma_0\, \Delta\lambda_D\, \pi F_\lambda \\ &\simeq \sigma_0\, (\Delta\lambda_\oplus/\Delta\lambda_\odot)\, \pi F \end{aligned} \qquad (2)$$

Here σ_0 is the resonance-scattering cross section at line center λ_0, $\Delta\lambda_D$ is the Doppler width of the scattering atoms/ions defined by $\Delta\lambda_D = \lambda_0 v_{th}/c$, πF_λ is the solar flux per unit wavelength at line center and πF is the total solar flux of the line. For emissions such as the 834Å line, for which the solar line profile is unknown, an estimate was made using a value of the Earth and solar Doppler width ratio $\Delta\lambda_\oplus/\Delta\lambda_\odot \sim 0.05$. Table 1 lists the total solar fluxes and estimated g-factors for line emissions. Cross sections used in Table 1 were calculated from oscillator strengths found in Wiese et al. [1966]; the solar fluxes were estimated from Heroux and Hinteregger [1978], and line shapes were estimated from Skelton [1978]. Recent solar models [D. Shemansky, private communications, 1989] suggest that perhaps most of the solar emission at 834Å results from a coincident O^{++} multiplet rather than from the O^+ 834Å triplet. The estimated g-factor for the 834Å line reflects this new information. If this suggestion proves not to be true, then the 834Å g-factor in Table 1 may have to be increased by perhaps a factor of ~ 10.

Simple models of O^+ and O^0 number densities have been used, based on observations and/or theory, with the contribution due to 'hot' outflowing ions and atoms ex-

Paper number 90GL00323.
0094-8276/90/90GL-00323$03.00

EXHIBIT 2

Title: Magnetospheric Imaging of High Latitude Ion Outflows

D.E. Garrido, R.M. Robinson, Y.T. Chiu, H.L. Collin

Lockheed Palo Alto Research Labortories, Palo Alto, CA

R.W. Smith and D.W. Swift

University of Alaska, Fairbanks, Alaska

Abstract:

Simulation of magnetospheric emissions from resonant scattering of sunlight by upward flowing He^+ (30.4 nm) and O^+ (83.4 nm) ions at high latitudes have been constructed for different satellite viewing locations and distances from the earth. The ion outflow data obtained by the Lockheed Ion Mass Spectrometer (EICS) on board the DE-1 spacecraft has been used to take into account the non-uniform distribution of ion flux intensities. For a polar orbiting satellite we obtain emission rates from outflowing ions of 5.2×10^{-2}R and 5.6×10^{-2}R for quiet and disturbed times for He^+ and 6.5×10^{-2}R and 7.5×10^{-2}R for quiet and disturbed times for 0^+, respectively. These low light levels are due to use of ion outflow data only. Emission levels from all ions can be quite a bit higher and awaits further data reduction from the Lockheed instrument. We find that an instrument field of view of at least 30^o is required at a distance of 9 R_E for images of the outflowing ions that exclude the bright emissions coming from plasmaspheric He^+ ions.

Because the O^+ intensities increase dramatically with magnetic activity, they represent a good signature of substorm-related processes. In our calculations we assume that the ions move along dipole magnetic field lines with a density profile that is modeled by a simple magnetic field scaling. The doppler shift of these moving ions modify the intensity of the resonantly scattered emissions. For He^+ the Doppler effects tend to decrease the intensities of the magnetospheric images while for O^+ at sufficiently high velocities the intensities may increase because enhanced scattering occurs.

EXHIBIT 3

Fabrication and Analysis of Mo-Si Multilayers

L. Shing, R.C. Catura

O/91-30, Bldg 256
Lockheed Palo Alto Research Laboratory
3251 Hanover St.
Palo Alto, CA 94304

ABSTRACT

Molybdenum-Silicon (Mo-Si) multilayers have been fabricated in our laboratory for reflecting various soft x-ray wavelengths. Several normal incidence mirrors have been produced for a solar sounding rocket flight. Using properly shaped masks on 3 inch diameter DC magnetrons, we can produce multilayers of a similar size having a uniformity of better than ±3% over their entire surface area. Peak reflectance of the multilayers are as high as 42% at 171Å. Efforts are underway to deposit several layers of different period on top of the multilayers in order to attenuate the reflection of 304Å, a very bright line of He II in the solar spectrum. In the interim, we have made a Mo-Si mirror that reflects at 304Å. In addition to obtaining information on the solar corona at this wavelength, this will greatly reduce the effects of the He II line when its image is appropriately subtracted from others. These results and a discussion of the current status of our multilayer research will be presented.

2. INTRODUCTION

We have been involved in fabricating multilayers for several years and our most recent experience is in depositing Molybdenum-Silicon multilayers on figured optical surfaces. First, the performance of various multilayer designs are studied by computer simulation to determine the optimal design for a selected wavelength, bandpass or angle of incidence. Step heights of each material are then deposited onto standard Si wafers to calibrate the deposition rates of the magnetrons. Proto-type multilayers are deposited onto Si wafers to confirm integrity of the design, and adequacy of the fabrication setup. The reflectance of the proto-types are then measured at various wavelengths, angles of incidence, and position on the test wafer. After optimizing the physical parameters, the actual flight optic is coated, and if practical, its reflectance is also measured. This paper describes our most recent experience in fabricating Mo-Si multilayer optics and presents data on their measured performance.

3. COMPUTER SIMULATION

We are able to calculate the reflectivities of various multilayer designs using a computer code developed by Dr. David Windt and his compilation of optical constants for a large number of materials. The code is able to compute the response of both periodic and nonperiodic multilayers. Figures 1 and 2 show the calculated reflectivities of multilayers designed for use in solar observations during an upcoming sounding rocket flight[1]. Parameters of the multilayer designs are indicated on the plots. The multilayer passband at 171Å is of interest to observe structure in the solar corona in an emission line of ionized Fe (Fe IX) that is formed at temperatures near 10^6 K. That at 195Å will be used to observe structure in a line of Fe XII formed at coronal temperatures near 2×10^6 K.

The computer simulations of the response of these multilayer designs show that their reflectivities at 304Å are about 5% of the reflectivities at the wavelengths of interest. This attenuation, however, is insufficient to reduce the contribution of an intense solar emission of He II at 304Å, which is about two orders of magnitude brighter than the two emission lines of interest. A possibility for further attenuating

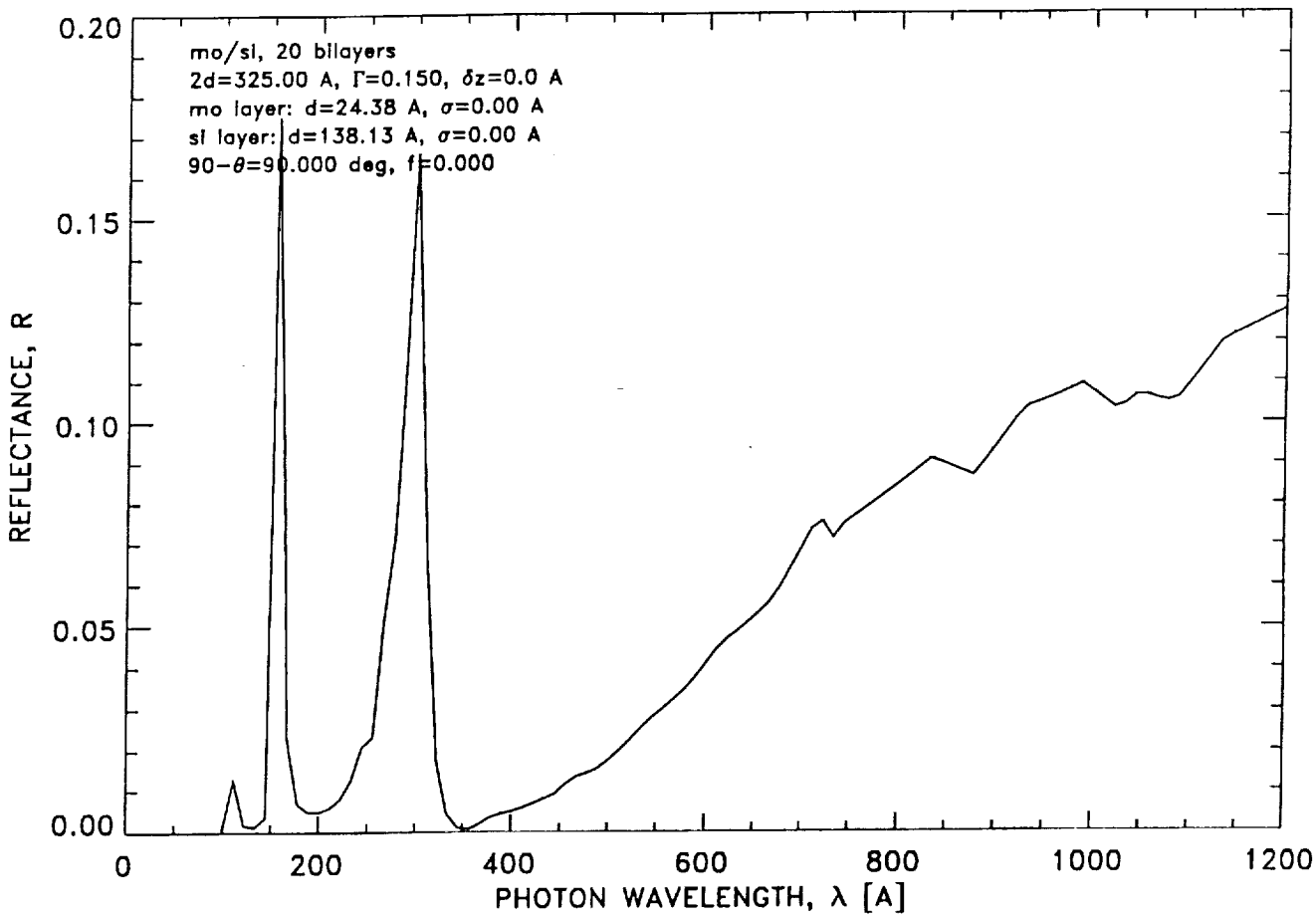
mo/si, 20 bilayers
2d=325.00 A, Γ=0.150, δz=0.0 A
mo layer: d=24.38 A, σ=0.00 A
si layer: d=138.13 A, σ=0.00 A
90−θ=90.000 deg, f=0.000
REFLECTANCE, R
0.20
0.15
0.10
0.05
0.00
0
200
400
600
800
1000
1200
PHOTON WAVELENGTH, λ [A]

EXHIBIT 4

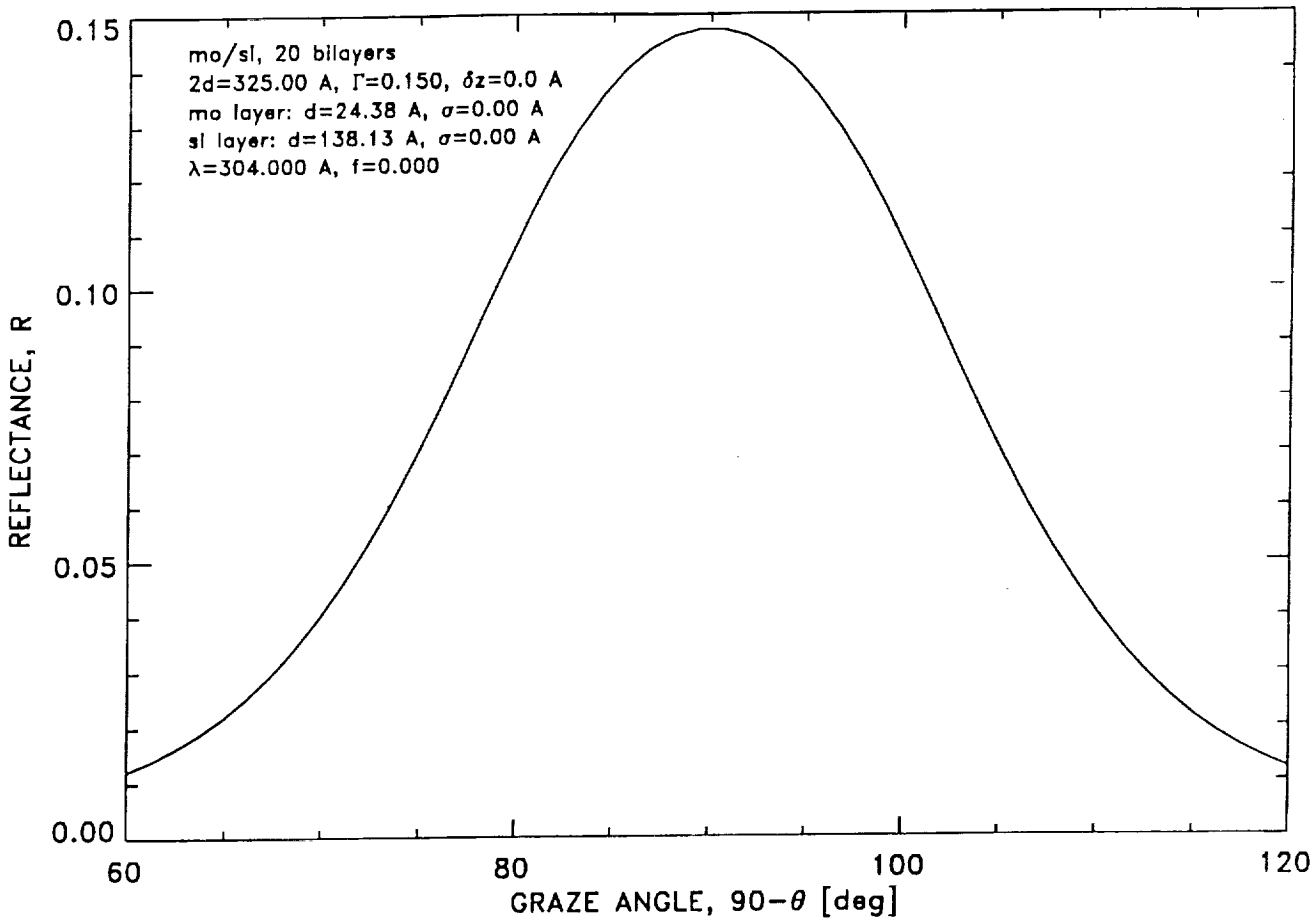
mo/si, 20 bilayers
2d=325.00 A, Γ=0.150, δz=0.0 A
mo layer: d=24.38 A, σ=0.00 A
si layer: d=138.13 A, σ=0.00 A
λ=304.000 A, f=0.000
REFLECTANCE, R
0.15
0.10
0.05
0.00
60
80
100
120
GRAZE ANGLE, 90−θ [deg]

EXHIBIT 5

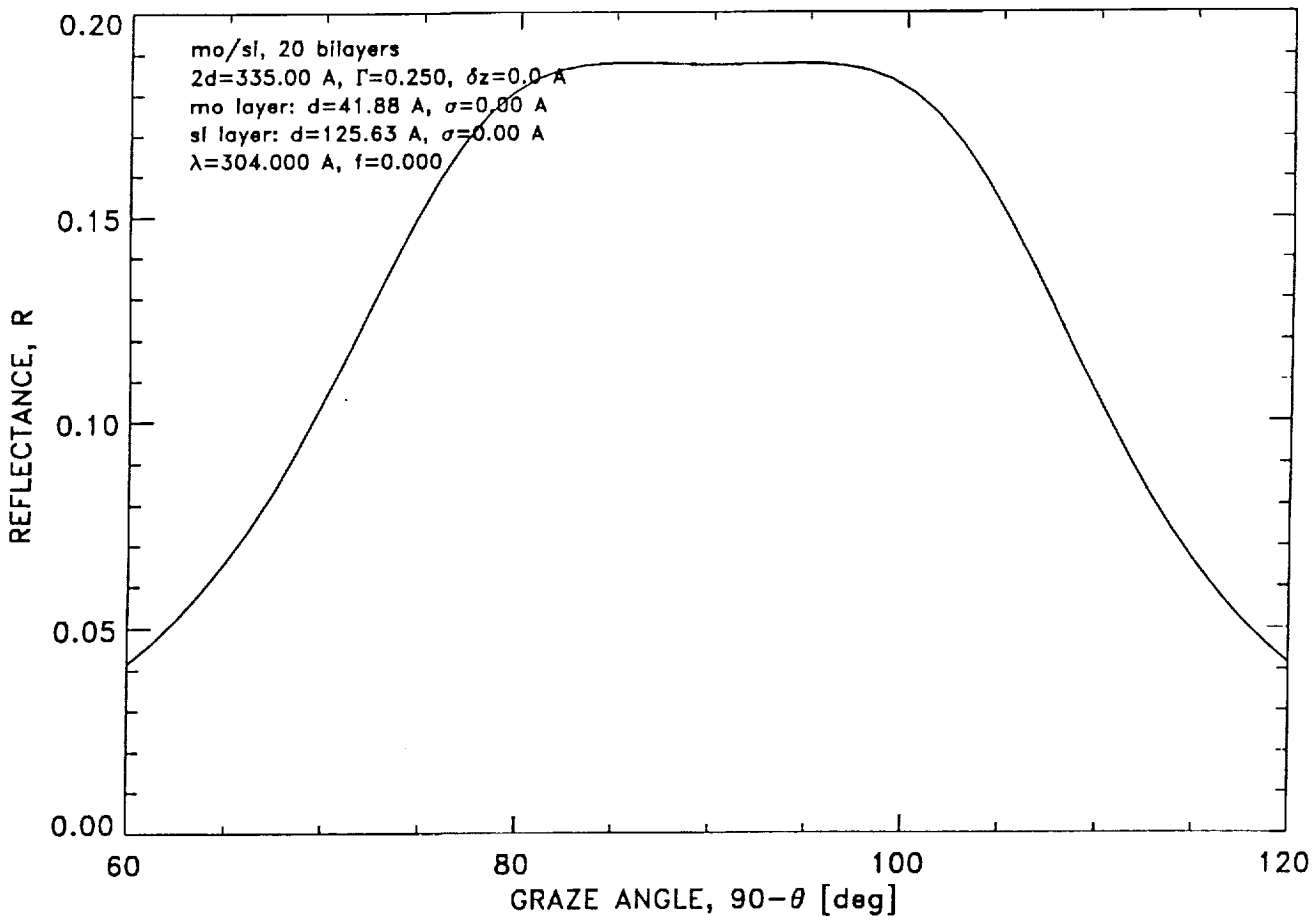
mo/si, 20 bilayers
2d=335.00 A, Γ=0.250, δz=0.0 A
mo layer: d=41.88 A, σ=0.00 A
si layer: d=125.63 A, σ=0.00 A
λ=304.000 A, f=0.000
REFLECTANCE, R
0.20
0.15
0.10
0.05
0.00
60
80
100
120
GRAZE ANGLE, 90−θ [deg]

EXHIBIT 6

LOCKHEED

R&DD

EFFECTS OF DOPPLER SHIFT ON RESONANCE SCATTERING

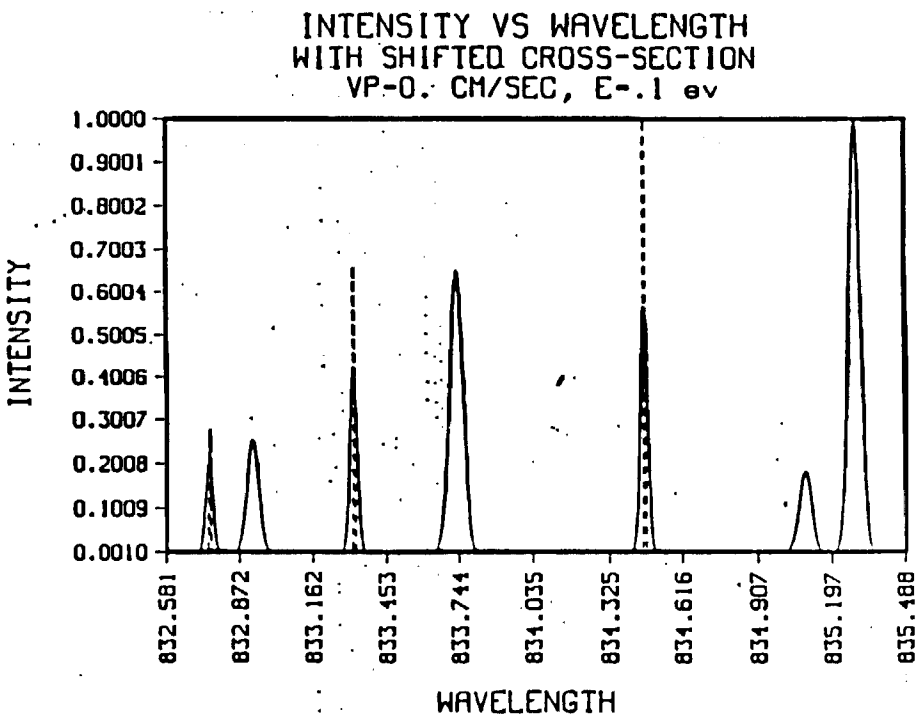

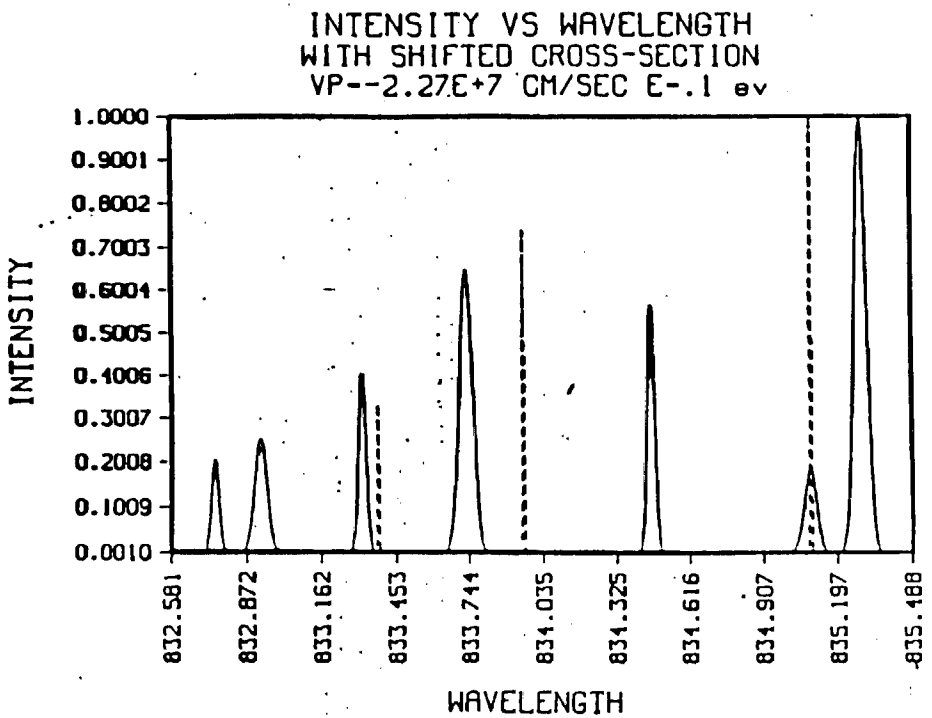

EXHIBIT 7

RESONANT SCATTERING FROM A GYRATING POPULATION

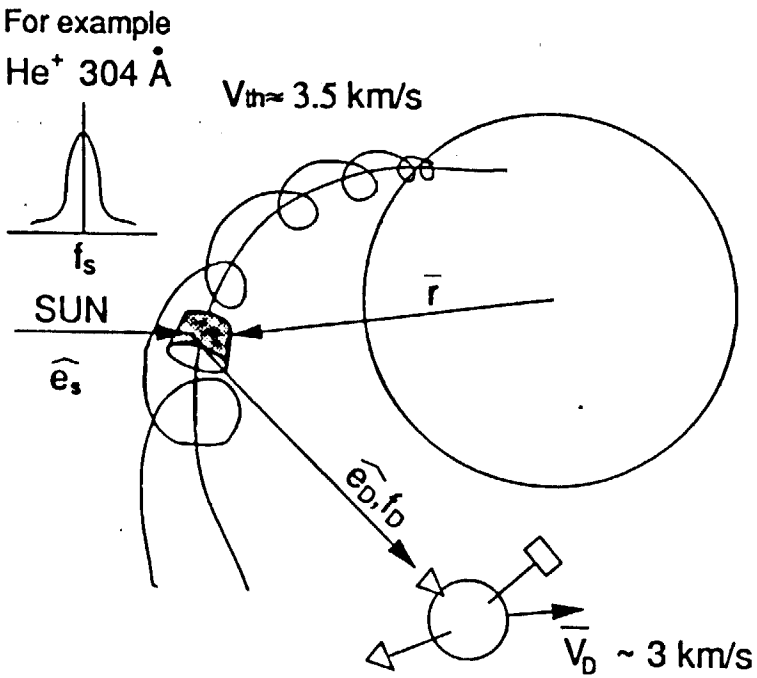

$\varepsilon(\bar{r},\hat{e_D},f_D)$ = Volume Emissivity (Photons $cm^{-2}s^{-1}sr^{-1}Hz^{-1}$)

$$= \frac{hf_o}{(4\pi)^2} B_{12} \int df_s \int R(\hat{e_s},f_s,\hat{e_D},f_o,\bar{v}) \cdot \pi F(f_s,\hat{e_s}) \left[n(\bar{r}) \left(\frac{m}{2\pi kT} \right)^{3/2} \exp\left(- \frac{mv^2}{2kT} \right) \right] d\bar{v}$$

f_o = frequency at center of resonance line

B_{12} = Einstein absorption coefficient from level 1 to level 2

πF = Solar Spectral Irradiance (photons $cm^{-2}s^{-1}Hz^{-1}$)

R = Hummer's Redistribution Function

Detected frequencies are Doppler Shifted : $f = f_D \left(1 + \frac{\bar{V_D}}{c} \cdot \hat{e_D} \right)$

EXHIBIT 8

NASA

Report Documentation Page

1. Report No.	2. Government Accession No.	3. Recipient's Catalog No.

4. Title and Subtitle

IMAGING THE MAGNETOSPHERE IN THE EXTREME ULTRAVIOLET

5. Report Date

Febuary 1993

6. Performing Organization Code

7. Author(s)

Y.T. Chiu

8. Performing Organization Report No.

10. Work Unit No.

9. Performing Organization Name and Address

LOCKHEED PALO ALTO RESEARCH LABORATORY
3251 Hanover Street, Palo Alto, CA 94304

11. Contract or Grant No.

NASW-4529

13. Type of Report and Period Covered

FINAL REPORT

12. Sponsoring Agency Name and Address

National Aeronautics and Space Administration
NASA Headquarters, Code SS
Washington, D.C. 20546-0001

14. Sponsoring Agency Code

15. Supplementary Notes

16. Abstract

This is the final report on 2.5 calendar years of contract research on magnetosphere imaging in the extreme ultraviolet. The objectives of the research contract can be summarized in three related items: (1). Investigate the feasibility of the EUV imaging concept by using Lockheed in-situ ion measurement data. (2). Investigate the technical resources required to make scientific interpretations of such EUV images by end-to-end simulations of the imaging concept. (3). Construct and test the key element for EUV magnetosphere imaging, the multilayer mirror with normal-incidence reflectance designed for the selected solar resonance line.

Researches as per contract have successfully fulfilled all three scientific objectives stated above. The body of this report emphasizes accomplishments in the second year. Accomplishments in the first year are summarized in the Annual Progress Report for 1991, which is included here as Appendix 1.

17. Key Words (Suggested by Author(s))

MAGNETOSPHERE
IMAGING
EXTREME ULTRAVIOLET

18. Distribution Statement

Unclassified - Unlimited

19. Security Classif. (of this report)	20. Security Classif. (of this page)	21. No. of pages	22. Price
U.	U.	24	

NASA FORM 1626 OCT 86